Title: Oral drug repositioning candidates and synergistic remdesivir combinations for the prophylaxis and treatment of COVID-19

Authors:

Malina A. Bakowski[1]†*, Nathan Beutler[2]†, Emily Chen[1], Tu-Trinh H. Nguyen[1], Melanie G. Kirkpatrick[1], Mara Parren[2], Linlin Yang[2], James Ricketts[2], Anil K. Gupta[1], Mitchell V. Hull[1], Peter G. Schultz[1], Dennis R. Burton[2], Arnab K. Chatterjee[1], Case W. McNamara[1], Thomas F. Rogers[2,3]*

Affiliations:

[1]Calibr, a division of The Scripps Research Institute, 11119 North Torrey Pines Road, La Jolla, CA 92037.

[2]Department of Immunology and Microbiology, The Scripps Research Institute, 10550 North Torrey Pines Road, La Jolla, CA 92037.

[3]UC San Diego Division of Infectious Diseases and Global Public Health, UC San Diego School of Medicine, La Jolla, CA 92093.

*Correspondence to: mbakowski@scripps.edu, trogers@scripps.edu.

†These authors contributed equally to this work.

Abstract:

The ongoing pandemic caused by the novel severe acute respiratory syndrome coronavirus 2 (SARS-CoV-2), necessitates strategies to identify prophylactic and therapeutic drug candidates for rapid clinical deployment. A high-throughput, high-content imaging assay of human HeLa cells expressing the SARS-CoV-2 receptor ACE2 was used to screen ReFRAME, a best-in-class drug repurposing library. From nearly 12,000 compounds, we identified 66 compounds capable of selectively inhibiting SARS-CoV-2 replication in human cells. Twenty-four of these drugs show additive activity in combination with the RNA-dependent RNA polymerase inhibitor remdesivir and may afford increased in vivo efficacy. We also identified synergistic interaction of the nucleoside analog riboprine and a folate antagonist 10-deazaaminopterin with remdesivir. Overall, seven clinically approved drugs (halofantrine, amiodarone, nelfinavir, simeprevir, manidipine, ozanimod, osimertinib) and 19 compounds in other stages of development may have the potential to be repurposed as SARS-CoV-2 oral therapeutics based on their potency, pharmacokinetic and human safety profiles.

Main Text:

In early December of 2019 the severe acute respiratory syndrome coronavirus 2 (SARS-CoV-2) was identified as the cause of rapidly increasing numbers of severe pneumonia-like symptoms termed COVID-19 [1]. Since then, SARS-CoV-2 has rightfully been given its pandemic status by the World Health Organization (WHO). As of May 4, SARS-CoV-2 has spread throughout the world causing a combined total of more than 3,407,000 confirmed infections and more than 238,000 reported deaths in 215 different countries [2]. Antiviral treatment options for COVID-19 are extremely limited. Many compounds, such as ribavirin, interferon, lopinavir-ritonavir, and corticosteroids that had been used in

patients with SARS-CoV-1 and MERS-CoV, remain unvalidated for the newly emerged SARS-CoV-2 [3]. Remdesivir, a nucleotide analog prodrug with broad antiviral activity that works as an RNA-dependent RNA polymerase inhibitor, has been reported to be effective against MERS-CoV and SARS-CoV-1 infections in animal models [4-6]. Repositioning of remdesivir as a treatment against SARS-CoV-2 infection has recently demonstrated positive clinical endpoints in a Phase 3 Adaptive COVID-19 Treatment Trial (median time to recovery shortened from 15 to 11 days) [7] that justified emergency use authorization of remdesivir by the US Food & Drug Administration for treatment of hospitalized COVID-19 patients [8]. The effectiveness of the repurposed drug remdesivir, with the current formulation requiring administration by IV infusion, both highlights the importance of investigating pre-existing drugs to combat SARS-CoV-2 infections, and the need for discovery of new or supplemental therapies that result in greater clinical improvements and can be administered outside of a hospital setting (i.e. orally). The ReFRAME (Repurposing, Focused Rescue, and Accelerated Medchem) drug collection is an extensive drug repurposing library containing nearly 12,000 small-molecule drugs shown to be appropriate for direct use in humans [9] and provides a rich resource to discover new treatments that may be used as additional monotherapies or even in combination with remdesivir to further enhance efficacy and reduce drug resistance potential.

High-throughput cell-based phenotypic assay against SARS-CoV-2

To identify compounds that could inhibit entry or replication of SARS-CoV-2 in human cells, we developed a high-content imaging (HCI) 384-well format assay using HeLa cells expressing the human SARS-CoV-2 receptor, the angiotensin-converting enzyme 2, or ACE2 (HeLa-ACE2). In this assay HeLa-ACE2 cells are infected with SARS-CoV-2 virus in the presence of compounds of interest, and viral infection is quantified 24 hours later (Fig. 1A). The assay relies on immunofluorescent detection of SARS-CoV-2 proteins with sera purified from patients exposed to the virus, which together with host cell nuclear staining allows for quantification of the percent infected cells in each well (Fig. 1B).

We validated the assay using compounds with reported activity against Ebola and suspected or previously verified activity against SARS-CoV-2: remdesivir (GS-5734) [10] ($EC_{50} = 194 \pm 20$ nM; average $\pm$ sem of 5 independent experiments) and the PIKfyve inhibitor apilimod ($EC_{50} = 50 \pm 11$ nM, average $\pm$ sem of 4 independent experiments) (Fig. 1B). Remdesivir at elevated concentrations was able to eliminate infected cells almost completely (Fig. 1C) and we used it at a concentration of 2.5 µM as a positive control, with data normalized to it and neutral DMSO control wells. While apilimod was more potent than remdesivir, it had a fractionally lower maximal efficacy (85-90% of uninfected cells at the highest effective concentrations) compared to remdesivir. Additionally, we assessed compound toxicity in the context of infection by quantifying the total cell numbers per well, with cytotoxic protein synthesis inhibitor puromycin as a positive control (average $EC_{50} = 547 \pm 27$ nM, average $\pm$ sem of 5 independent experiments; HeLa-ACE2 $CC_{50} = 2.45 \pm 0.23$ µM, average $\pm$ sem of 5 independent experiments). Notably, a concomitant increase in cell numbers coincided with the antiviral activity of remdesivir and apilimod, likely due to reduction in proliferation of infected cells (Fig. 1B-E). Altering the multiplicity of infection had modest effects on the potency of control compounds in the same experiment, with a 2.7-fold increase in remdesivir's EC_{50} from MOI=1 to MOI=26, and a 3.7-fold increase in apilimod's EC_{50}, but not that of puromycin (Fig. S1).

Using the developed assay, we ran a pilot screen to assess the activity of 148 small molecules with suspected therapeutic potential against coronavirus infections mined from the available literature [11] (RZ' = 0.84). We identified 19 compounds with an $EC_{50} < 9.6$ µM and, based on data obtained from an uninfected HeLa-ACE2 24-hour live/dead assay, 10 of these were selective (uninfected HeLa-ACE2

CC_{50}/SARS-CoV-2 $EC_{50} > 10$ or uninfected HeLa-ACE2 $CC_{50} > 40$ µM) (Table S1). This included library/screening lots of apilimod ($EC_{50} = 184$ nM, $CC_{50} > 40$ µM) and remdesivir ($EC_{50} = 300$ nM $CC_{50} > 40$ µM) that were "rediscovered" in the assay. The higher EC_{50} of apilimod and remdesivir are likely due to slight degradation over time in the screening deck compared to freshly prepared control powder stock.

Screening ReFRAME, a best-in-class drug repurposing library

Next, we screened the 12,000-compound ReFRAME repurposing library at a final concentration of 1.9 µM and 9.6 µM. Assay quality was maintained throughout both screens (RZ' of 0.87 and 0.72, respectively) (Table 1) and a clear distinction was apparent in the activity profiles of DMSO vehicle- (neutral control), remdesivir- (positive control), apilimod-, and puromycin- (toxicity control)-treated wells (Fig. 1D, 1E). Hits were selected based on demonstration of >50% reduction in the number of infected cells per well (<-50% activity normalized to neutral controls minus inhibitors) and <40% toxicity based on the total cell number per well (>-40% activity normalized to compound activities, including 10 µM puromycin) (Fig, 1E, 1F) identifying 61 primary hits at 1.9 µM and 266 primary hits at 9.6 µM screening concentrations (hit rates of 0.51 and 2.24%, respectively), with a total of 311 hits.

The hit rate for the primary screen of the ReFRAME library was high (2.75%), but not unexpected for this collection of bioactive small molecules, many of which are approved drugs or in clinical phases of development and used for a wide assortment of indications (Fig. 2A). To reconfirm and assess potency and selectivity of the primary hits we tested 310 of the available compounds in a 10-point 1:3 dilution dose response format with a top concentration of 9.6 µM. Of these, 225 (72.6%) demonstrated activity with $EC_{50} < 9.6$ µM against SARS-CoV-2. However, many of the primary screen hits were also cytotoxic, with an unacceptably low selectivity ratio as determined in uninfected HeLa-ACE2 cells (uninfected CC_{50}/$EC_{50} < 10$) (Table 2, Fig. 2B). Because viruses rely on host machinery for replication, it was not unexpected that many of the compounds with antiviral activity also affected vital host processes. Interestingly, this toxicity was sometimes masked in infected cells, as reduction of viral infection by compounds like the protein synthesis inhibitor puromycin and even hydroxychloroquine provided a benefit to cell health in the context of infection but not in uninfected cells (Fig. 2C, Table S1).

Between the small pilot and the ReFRAME screen, and not including remdesivir, we identified 67 (66 unique as two different lots of GW-803430 were identified) potent ($EC_{50} < 9.6$ µM) and selective (CC_{50}/$EC_{50} > 10$ or $CC_{50} > 39.8$ µM) compounds (Fig. 2B, D, Table S1). The top four classes of potent and selective compounds were oncolytic compounds, ion channel modulators, anti-psychotics and receptor binding compounds (Fig. 2D). A fifth of potent and selective hits could be classified as oncolytic drugs, further reflecting the reliance of the virus on host cell processes present in rapidly proliferating cells. The identification of compounds belonging to anti-psychotic, cardiovascular, and even anti-parasitic (neglected tropical diseases) classes may reflect the cationic amphiphilic nature of some of these molecules and their ability to accumulate in and impact acidic intracellular compartments (e.g. late endosomes/lysosomes). Resultant dysregulation of the endo-lysosomal pathway and lipid homeostasis has been suggested to impair viral entry and/or replication [12] and this mode of action has been speculated for amiodarone and hydroxychloroquine, both identified here as potent and selective hits against SARS-CoV-2 in our screen (Table 2, Table S1). We also identified two selective estrogen receptor modulators (bazedoxifene, $EC_{50} = 3.47$ µM and raloxifene $EC_{50} = 4.13$ µM); a class of compounds previously found to inhibit Ebola virus infection [13].

Out of the identified hits, of highest interest were the newly identified approved oral drugs halofantrine HCl, amiodarone, nelfinavir mesylate, simperevir, manidipine, ozanimod andosimertinib, due to their relatively high exposures or a long history of use as therapeutic agents and therefore potential to be quickly repurposed as COVID-19 treatments following further efficacy vetting in animal models. The viral protease inhibitors nelfinavir and simeprevir have good exposures and based on their described mode of action we speculate that they inhibit SARS-CoV-2 directly. The selective sphingosine-1-phosphate (S1P1) receptor modulator ozanimod is also intriguing as a potential COVID-19 therapy. Selective S1P1 agonists have been shown to provide significant protection against influenza virus infection in murine models by reducing inflammation at the site of infection (reducing release of cytokines by pulmonary endothelial cells and infiltration of lymphocytes into the lungs) [14], and thus ozanimod may serve as a good combination partner for a direct-acting antiviral drug. The approved calcium-channel blocker manidipine has low exposure but may have the potential to improve COVID-19 disease outcomes for patients. Interestingly, amiodarone has previously been identified as having broad-spectrum antiviral activity in an in vitro screen [15]. Nineteen other compounds in various stages of development such as apilimod (assay control that may inhibit viral entry through disruption of endo-lysosomal trafficking, as found for filoviruses[16]), the protease inhibitors NCO 700 (cathepsin B) and dutacatib (cathepsin K), which may also impact viral entry, all have the potential to show efficacy due to their potency or pharmacokinetic profiles (Table 2). Most of these, except for the very potent apilimod, had modest $EC_{50}s > 1$ µM that did not surpass the potency of remdesivir. However, remdesivir's requirement for intravenous administration and potentially limited efficacy warrants further investigation into alternative or supplemental therapies. Therefore, we investigated whether the hits identified in our screen would be suitable as partners for a combination therapy with remdesivir.

Combination therapies

Combination therapies have the potential to increase efficacy of treatment while reducing drug dose of either or both combinations partners, and thus prevent side effects that may be associated with administration of higher doses. Drug combinations can also slow the acquisition of drug resistance. Drug synergy, the increase in activity of the combination therapy beyond what is expected of an additive interaction is rare, yet additive effects themselves have the potential to improve therapy regimens. Conversely, antagonism, the inhibition of activity of the overall combination beyond what would be expected if the compounds acted independently, is an undesirable property. To identify synergistic, additive, and antagonistic interactions between remdesivir and ReFRAME hits, we performed synergy interactions studies in a checkerboard experiment, comparing full dose response of remdesivir against the dose responses of 24 hits with attractive safety and pharmacokinetic profiles in a 10×10 matrix (Fig. 2E). We used the *synergyfinder* package [17] in R to assess the interactions between the tested compounds using the Zero Interaction Potency Model (ZIP) [18], where a δ score > 10 indicates likely synergy, δ < -10 indicates antagonism, and δ between -10 and 10 suggests an additive interaction. We found no genuine synergy between remdesivir and the compounds tested; however, the combinations were additive, including that of nelfinavir with remdesivir (Fig. 3A, Table 1, Table S1), suggesting these drugs, if they were to prove efficacious in vivo, could potentially be co-administered with remdesivir to increase the overall safety and efficacy of treatment, while limiting the evolution of drug resistance.

To identify compounds that interact synergistically with remdesivir we carried out a second unbiased ReFRAME screen in the presence of low concentrations (80 nM) of remdesivir. The activity of novel hits from this screen were assessed in the presence and absence of remdesivir. Based on a perceived shift in activity in the presence of remdesivir, compounds were tested in a checkerboard

synergy matrix and we identified the nucleoside analog riboprine (N6-isopentenyladenosine, previously investigated as an antineoplastic agent, for treatment of nausea and surgical site infections, and a component of CitraNatal 90 DHA, a prescription prenatal/postnatal multivitamin/mineral tablet) and a folate antagonist 10-deazaaminopterin (an antineoplastic compound currently in Phase II stage of development) as having activities that synergized with those of remdesivir. The synergistic effects for both compounds were observed across specific concentrations, signified as peaks within the 3-dimensional synergy score landscape (Figure 3B, 3C), prompting closer scrutiny of activity of each compound. Riboprine achieved maximal (100%) efficacy over the range of concentrations tested, but addition of EC_2 of remdesivir shifted its EC_{50} from 12 µM to 3.6 µM, and addition of EC_{24} of remdesivir increased its potency further to $EC_{50} = 1.6$ µM (Figure 3B). 10-deazaaminopterin showed only 40% maximal efficacy over the range of concentrations tested, but the addition of EC_2 of remdesivir caused an increase of maximal efficacy from 40% to nearly 65% (where a shift of 2% would be expected) and addition of EC_{24} of remdesivir increased maximal efficacy of the combination from 40% to >80% (Figure 3C). The mechanism of action behind the observed synergies remains to be determined. Riboprine has been reported to block uridine and cytidine import[19] and through inhibition of protein prenylation to inhibit autophagy[20] which could impact RNA catabolism[21] whereas 10-deazaaminopterin has been suggested to inhibit folate dependent enzymes of the purine biosynthesis pathway[19-22]. Therefore, treatment with either riboprine or 10-deazaaminopterin may result in reduced intracellular nucleoside pools and in this way synergize with RdRp inhibition by the adenosine nucleoside analog remdesivir. However, another or more direct and specific interaction cannot be excluded and remains to be elucidated. While these findings indicate a promising avenue for further investigation of combination therapies for treatment of COVID-19, the adverse effects of these agents (e.g. inhibition of immunity by 10-deazaaminopterin) would need to be carefully considered in the design and dose selection of in vivo validation experiments.

In summary, by screening the high-value repurposing ReFRAME library we identified 75 unique known drugs or preclinical molecules with activity against SARS-CoV-2 in human cells, 24 of which were tested and showed an additive interaction in combination with the antiviral compound remdesivir recently granted emergency approval for treatment of SARS-CoV-2 infection. We also identified a synergistic interaction between remdesivir and both 10-deazaaminopterin and riboprine. Our data support the advancement of the identified compounds for further profiling in in vivo models to assess their utility (alone or in combination with remdesivir) in combating the COVID-19 pandemic.

Methods

Virus generation

Vero E6 cells (ATCC CRL-1586) were plated in a T225 flask with complete DMEM (Corning 15-013-CV) containing 10% FBS, 1×PenStrep (Corning 20-002-CL), 2 mM L-Glutamine (Corning 25-005-CL) overnight at 37□ 5% CO_2. The media in the flask was removed and 2 mL of SARS-CoV-2 strain USA-WA1/2020 (BEI Resources NR-52281) in complete DMEM was added to the flask at an MOI of 0.5 and was allowed to incubate for 30 minutes at 34□ 5% CO_2. After incubation, 30 mL of complete DMEM was added to the flask. The flask was then placed in a 34□ incubator at 5% CO_2 for 5 days. On day 5 post infection the supernatant was harvested and centrifuged at 1,000×g for 5 minutes. The supernatant was filtered through a 0.22 µM filter and stored at -80□.

The ReFRAME library: Compound management, drug annotation and screen data access

The ReFRAME library collection consists of nearly 12,000 high-purity compounds (>95%) dissolved in high-quality dimethyl sulfoxide (DMSO). Compound quality control was performed by liquid chromatography-mass spectrometry and/or ^{1}H-NMR when required. The library was prepared at two concentrations, 2 and 10 mM, to support low-concentration (2–10 µM) and high-concentration (10–50 µM) screening formats. Echo-qualified 384-well low dead volume plus microplates (LP-0200-BC; Labcyte Inc.) were used as the library source plates to support acoustic transfer with an Echo 555 Liquid Handler (Labcyte Inc.). Compounds not soluble in DMSO were plated in water (129 compounds); compounds lacking long-term solubility in DMSO were suspended just before dispensing to avoid precipitation (71 compounds). Additional details available at https://reframedb.org/about.

Associated compound annotation are supported by three widely used commercial drug competitive intelligence databases: Clarivate Integrity, GVK Excelra GoStar, and Citeline Pharmaprojects. As available, annotation data may include status of clinical development and highest stage of development achieved, mechanism of action, drug indication(s), and route of administration.

In accordance with ReFRAME data policies, open access to these data are assured and have been expedited for immediate disclosure at https://reframedb.org/.

HeLa-ACE2 stable cell line

HeLa-ACE2 cells were generated through transduction of human ACE2 lentivirus. The lentivirus was created by co-transfection of HEK293T cells with pBOB-hACE2 construct and lentiviral packaging plasmids pMDL, pREV, and pVSV-G (Addgene) using Lipofectamine 2000 (Thermo Fisher Scientific, 11668019). Supernatant was collected 48 h after transfection then used to transduce pre-seeded HeLa cells. 12 h after transduction stable cell lines were collected, scaled up and stored. Cells were maintained in DMEM (Gibco, 11965-092) with 10% FBS (Gibco, 10438026) and 1× sodium pyruvate (Gibco, 11360070) at 37□ 5% CO_2.

SARS-CoV-2/HeLa-ACE2 high-content screening assay

Compounds were acoustically transferred into 384-well µclear-bottom plates (Greiner, Part. No. 781090-2B). HeLa-ACE2 cells were seeded in 13 µL DMEM with 2% FBS at a density of $1.0{\times}10^3$ cells per well. Plated cells were transported to the BSL3 facility where 13 µL of SARS-CoV-2 diluted in assay media was added per well at a concentration of $2.0{\times}10^6$ PFU/mL (assay multiplicity of infection (MOI) = 2.2). Plates were incubated for 24 h at 34□ 5% CO_2, and then fixed with 25 µL of 8% formaldehyde for 1 h at 34□ 5% $CO_2.$ Plates were washed with 1xPBS 0.05% Tween 20 in between fixation and subsequent primary and secondary antibody staining. Human polyclonal sera diluted 1:500 in Perm/Wash buffer (BD Biosciences 554723) was added to the plate and incubated at RT for 2 h. Six µg/mL of goat anti-human H+L conjugated Alexa 488 (Thermo Fisher Scientific A11013) together with 8 µM of antifade-46-diamidino-2-phenylindole (DAPI; Thermo Fisher Scientific D1306) in SuperBlock T20 (PBS) buffer (Thermo Fisher Scientific 37515) was added to the plate and incubated at RT for 1 h in the dark. Plates were imaged using the ImageXpress Micro Confocal High-Content Imaging System (Molecular Devices) with a 10× objective, with 4 fields imaged per well. Images were analyzed using the Multi-Wavelength Cell Scoring Application Module (MetaXpress), with DAPI staining identifying the host-cell nuclei (the total number of cells in the images) and the SARS-CoV-2 immunofluorescence signal leading to identification of infected cells.

Uninfected host cell cytotoxicity counter screen

Compounds were acoustically transferred into 1,536-well μclear plates (Greiner Part. No. 789091). HeLa-ACE2 cells were maintained as described for the infection assay and seeded in the assay-ready plates at 400 cells/well in DMEM with 2% FBS and plates were incubated for 24 hours at 37▯ 5% CO_2. To assess cell viability, the Image-iT DEAD green reagent (Thermo Fisher) was used according to manufacturer instructions. Cells were fixed with 4% paraformaldehyde, and counterstained with DAPI. Fixed cells were imaged using the ImageXpress Micro Confocal High-Content Imaging System (Molecular Devices) with a 10× objective, and total live cells per well quantified in the acquired images using the Live Dead Application Module (MetaXpress).

Data analysis

Image analysis was carried out with MetaXpress (version 6.5.4.532). Primary in vitro screen and the host cell cytotoxicity counter screen data were uploaded to Genedata Screener, Version 16.0.3-Standard. Data were normalized to neutral (DMSO) minus inhibitor controls (2.5 μM remdesivir for antiviral effect and 10 μM puromycin for infected host cell toxicity). For the uninfected host cell cytotoxicity counter screen 40 μM puromycin (Sigma) was used as the positive control. For dose response experiments compounds were tested in technical triplicates on different assay plates and dose curves were fitted with the four parameter Hill Equation. Technical replicate data were analyzed using median condensing. The *synergyfinder* package[17] in R (version 3.6.3) was used for synergy analysis.

Data availability

All data are available in the main text or the supplementary materials. Results from the screen of the ReFRAME library have been deposited to the reframedb.org data portal.

References:

1   Huang, C. *et al.* Clinical features of patients infected with 2019 novel coronavirus in Wuhan, China. *Lancet* **395**, 497-506, doi:10.1016/S0140-6736(20)30183-5 (2020).
2   Organization, W. H. Vol. 2020 (ed World Health Organization) (World Health Organization, 2020).
3   Zumla, A., Chan, J. F., Azhar, E. I., Hui, D. S. & Yuen, K. Y. Coronaviruses - drug discovery and therapeutic options. *Nat Rev Drug Discov* **15**, 327-347, doi:10.1038/nrd.2015.37 (2016).
4   de Wit, E. *et al.* Prophylactic and therapeutic remdesivir (GS-5734) treatment in the rhesus macaque model of MERS-CoV infection. *Proc Natl Acad Sci U S A* **117**, 6771-6776, doi:10.1073/pnas.1922083117 (2020).
5   Sheahan, T. P. *et al.* Broad-spectrum antiviral GS-5734 inhibits both epidemic and zoonotic coronaviruses. *Sci Transl Med* **9**, doi:10.1126/scitranslmed.aal3653 (2017).
6   Lo, M. K. *et al.* GS-5734 and its parent nucleoside analog inhibit Filo-, Pneumo-, and Paramyxoviruses. *Sci Rep* **7**, 43395, doi:10.1038/srep43395 (2017).
7   Health, N. I. o.   (2020).
8   Administration, U. S. F. D.   (ed U.S. Food & Drug Administration) (U.S. Food & Drug Administration, 2020).
9   Janes, J. *et al.* The ReFRAME library as a comprehensive drug repurposing library and its application to the treatment of cryptosporidiosis. *Proc Natl Acad Sci U S A* **115**, 10750-10755, doi:10.1073/pnas.1810137115 (2018).

10   Wang, M. *et al.* Remdesivir and chloroquine effectively inhibit the recently emerged novel coronavirus (2019-nCoV) in vitro. *Cell Res* **30**, 269-271, doi:10.1038/s41422-020-0282-0 (2020).

11   Prajapat, M. *et al.* Drug targets for corona virus: A systematic review. *Indian J Pharmacol* **52**, 56-65, doi:10.4103/ijp.IJP_115_20 (2020).

12   Salata, C., Calistri, A., Parolin, C., Baritussio, A. & Palu, G. Antiviral activity of cationic amphiphilic drugs. *Expert Rev Anti Infect Ther* **15**, 483-492, doi:10.1080/14787210.2017.1305888 (2017).

13   Johansen, L. M. *et al.* FDA-approved selective estrogen receptor modulators inhibit Ebola virus infection. *Sci Transl Med* **5**, 190ra179, doi:10.1126/scitranslmed.3005471 (2013).

14   Oldstone, M. B., Teijaro, J. R., Walsh, K. B. & Rosen, H. Dissecting influenza virus pathogenesis uncovers a novel chemical approach to combat the infection. *Virology* **435**, 92-101, doi:10.1016/j.virol.2012.09.039 (2013).

15   Mazzon, M. *et al.* Identification of Broad-Spectrum Antiviral Compounds by Targeting Viral Entry. *Viruses* **11**, doi:10.3390/v11020176 (2019).

16   Nelson, E. A. *et al.* The phosphatidylinositol-3-phosphate 5-kinase inhibitor apilimod blocks filoviral entry and infection. *PLoS Negl Trop Dis* **11**, e0005540, doi:10.1371/journal.pntd.0005540 (2017).

17   Ianevski, A., He, L., Aittokallio, T. & Tang, J. SynergyFinder: a web application for analyzing drug combination dose-response matrix data. *Bioinformatics* **33**, 2413-2415, doi:10.1093/bioinformatics/btx162 (2017).

18   Yadav, B., Wennerberg, K., Aittokallio, T. & Tang, J. Searching for Drug Synergy in Complex Dose-Response Landscapes Using an Interaction Potency Model. *Comput Struct Biotechnol J* **13**, 504-513, doi:10.1016/j.csbj.2015.09.001 (2015).

19   Hakala, M. T., Slocum, H. K. & Gryko, G. J. N6-(delta2-isopentenyl)adenosine, an inhibitor of cellular transport of uridine and cytidine. *J Cell Physiol* **86**, 281-291, doi:10.1002/jcp.1040860212 (1975).

20   Ranieri, R. *et al.* N6-isopentenyladenosine dual targeting of AMPK and Rab7 prenylation inhibits melanoma growth through the impairment of autophagic flux. *Cell Death Differ* **25**, 353-367, doi:10.1038/cdd.2017.165 (2018).

21   Frankel, L. B., Lubas, M. & Lund, A. H. Emerging connections between RNA and autophagy. *Autophagy* **13**, 3-23, doi:10.1080/15548627.2016.1222992 (2017).

22   Baggott, J. E. *et al.* Antifolates in rheumatoid arthritis: a hypothetical mechanism of action. *Clin Exp Rheumatol* **11 Suppl 8**, S101-105 (1993).

23   Agency, E. M.   (ed Human Medicines Division) (European Medicines Agency, The Netherlands, 2020).

24   Morita, S., Takahashi, T., Yoshida, Y. & Yokota, N. Population Pharmacokinetics of Hydroxychloroquine in Japanese Patients With Cutaneous or Systemic Lupus Erythematosus. *Ther Drug Monit* **38**, 259-267, doi:10.1097/FTD.0000000000000261 (2016).

25   Porter, C. J. *et al.* Use of in vitro lipid digestion data to explain the in vivo performance of triglyceride-based oral lipid formulations of poorly water-soluble drugs: studies with halofantrine. *J Pharm Sci* **93**, 1110-1121, doi:10.1002/jps.20039 (2004).

26   Milton, K. A., Edwards, G., Ward, S. A., Orme, M. L. & Breckenridge, A. M. Pharmacokinetics of halofantrine in man: effects of food and dose size. *Br J Clin Pharmacol* **28**, 71-77, doi:10.1111/j.1365-2125.1989.tb03507.x (1989).

27   Emami, J. Comparative in vitro and in vivo evaluation of three tablet formulations of amiodarone in healthy subjects. *Daru* **18**, 193-199 (2010).

28   dos Santos Filho, H. O. *et al.* Comparative bioavailability study with two amiodarone tablet formulations administered with and without food in healthy subjects. *Arzneimittelforschung* **57**, 582-590, doi:10.1055/s-0031-1296653 (2007).

29   Pellegrin, I. *et al.* Virologic response to nelfinavir-based regimens: pharmacokinetics and drug resistance mutations (VIRAPHAR study). *AIDS* **16**, 1331-1340, doi:10.1097/00002030-200207050-00004 (2002).

30   Moyle, G. J. *et al.* Safety, pharmacokinetics, and antiretroviral activity of the potent, specific human immunodeficiency virus protease inhibitor nelfinavir: results of a phase I/II trial and extended follow-up in patients infected with human immunodeficiency virus. *J Clin Pharmacol* **38**, 736-743, doi:10.1002/j.1552-4604.1998.tb04814.x (1998).

31   Snoeys, J., Beumont, M., Monshouwer, M. & Ouwerkerk-Mahadevan, S. Mechanistic understanding of the nonlinear pharmacokinetics and intersubject variability of simeprevir: A PBPK-guided drug development approach. *Clin Pharmacol Ther* **99**, 224-234, doi:10.1002/cpt.206 (2016).

32   Reesink, H. W. *et al.* Rapid HCV-RNA decline with once daily TMC435: a phase I study in healthy volunteers and hepatitis C patients. *Gastroenterology* **138**, 913-921, doi:10.1053/j.gastro.2009.10.033 (2010).

33   Stockis, A. *et al.* Pharmacokinetics and tolerability of a new manidipine and delapril fixed oral combination in young and elderly subjects. *Arzneimittelforschung* **53**, 554-561, doi:10.1055/s-0031-1297149 (2003).

34   Stockis, A. *et al.* Single oral dose pharmacokinetic interaction study of manidipine and delapril in healthy volunteers. *Arzneimittelforschung* **53**, 627-634, doi:10.1055/s-0031-1297159 (2003).

35   Tran, J. Q. *et al.* Results From the First-in-Human Study With Ozanimod, a Novel, Selective Sphingosine-1-Phosphate Receptor Modulator. *J Clin Pharmacol* **57**, 988-996, doi:10.1002/jcph.887 (2017).

36   Kiura, K. *et al.* Osimertinib in patients with epidermal growth factor receptor T790M advanced non-small cell lung cancer selected using cytology samples. *Cancer Sci* **109**, 1177-1184, doi:10.1111/cas.13511 (2018).

37   Planchard, D. *et al.* Osimertinib Western and Asian clinical pharmacokinetics in patients and healthy volunteers: implications for formulation, dose, and dosing frequency in pivotal clinical studies. *Cancer Chemother Pharmacol* **77**, 767-776, doi:10.1007/s00280-016-2992-z (2016).

38   Salva, P., Costa, J., Perez-Campos, A. & Martinez-Tobed, A. Repeated dose pharmacokinetics of pancopride in human volunteers. *Biopharm Drug Dispos* **15**, 643-651, doi:10.1002/bdd.2510150803 (1994).

39   Harb Wael A, D. C. S., Lakhani Nehal, Rutherford Sarah C, Schreeder Marshall T, Ansell Stephen M, Sher Taimur, Aboulafia David M, Cohen Jonathon B, Nix Darrell, Landrette Sean, Flanders Kate, Miller Langdon L, Lichenstein Henri , Abramso Jeremy S. Phase 1 Clinical Safety, Pharmacokinetics (PK), and Activity of Apilimod Dimesylate (LAM-002A), a First-in-Class Inhibitor of Phosphatidylinositol-3-Phosphate 5-Kinase (PIKfyve), in Patients with Relapsed or Refractory B-Cell Malignancies. *ASH Annual Meeting 2017* **December 9-12 Atlatnta, GA, USA**.

40   Mzayek, F. *et al.* Randomized dose-ranging controlled trial of AQ-13, a candidate antimalarial, and chloroquine in healthy volunteers. *PLoS Clin Trials* **2**, e6, doi:10.1371/journal.pctr.0020006 (2007).

41   Patnaik, A. *et al.* A First-in-Human Phase I Study of the Oral p38 MAPK Inhibitor, Ralimetinib (LY2228820 Dimesylate), in Patients with Advanced Cancer. *Clin Cancer Res* **22**, 1095-1102, doi:10.1158/1078-0432.CCR-15-1718 (2016).

42   Doi, T. *et al.* Phase 1 pharmacokinetic study of the oral pan-AKT inhibitor MK-2206 in Japanese patients with advanced solid tumors. *Cancer Chemother Pharmacol* **76**, 409-416, doi:10.1007/s00280-015-2810-z (2015).

43   Wnuk-Lipinska Katarzyna, T. C., Gausdal Gro, Sandal Tone, Frink Robin, Hinz Stefan, Hellesøy Monica, Ahmed Lavina, Haugen Hallvard, Liang Xiao, Blø Magnus, Micklem David, Yule Murray, Minna John, Zhou Longen, Brekken Rolf, Lorens James. BGB324, a selective small molecule Axl kinase inhibitor to overcome EMT-associated drug resistance in carcinomas: Therapeutic rationale and early clinical studies. . *Proceedings of the 105th Annual Meeting of the American Association for Cancer Research* **2014 Apr 5-9**, doi:10.1158/1538-7445.AM2014-1747 (2014).

44   Song, N., Zhang, S., Li, Q. & Liu, C. Establishment of a liquid chromatographic/mass spectrometry method for quantification of tetrandrine in rat plasma and its application to pharmacokinetic study. *J Pharm Biomed Anal* **48**, 974-979, doi:10.1016/j.jpba.2008.06.002 (2008).

45   Stearns, R. A. *et al.* The pharmacokinetics of a thiazole benzenesulfonamide beta 3-adrenergic receptor agonist and its analogs in rats, dogs, and monkeys: improving oral bioavailability. *Drug Metab Dispos* **30**, 771-777, doi:10.1124/dmd.30.7.771 (2002).

46   Mathvink, R. J. *et al.* Discovery of a potent, orally bioavailable beta(3) adrenergic receptor agonist, (R)-N-[4-[2-[[2-hydroxy-2-(3-pyridinyl)ethyl]amino]ethyl]phenyl]-4-[4 -[4-(trifluoromethyl)phenyl]thiazol-2-yl]benzenesulfonamide. *J Med Chem* **43**, 3832-3836, doi:10.1021/jm000286i (2000).

47   Naryshkin, N. A. *et al.* Motor neuron disease. SMN2 splicing modifiers improve motor function and longevity in mice with spinal muscular atrophy. *Science* **345**, 688-693, doi:10.1126/science.1250127 (2014).

48   Patel, L. *et al.* Discovery of Orally Efficacious Phosphoinositide 3-Kinase delta Inhibitors with Improved Metabolic Stability. *J Med Chem* **59**, 9228-9242, doi:10.1021/acs.jmedchem.6b01169 (2016).

49   Washburn, W. N. *et al.* Identification of a nonbasic melanin hormone receptor 1 antagonist as an antiobesity clinical candidate. *J Med Chem* **57**, 7509-7522, doi:10.1021/jm500026w (2014).

50   Hertzog, D. L. *et al.* The discovery and optimization of pyrimidinone-containing MCH R1 antagonists. *Bioorg Med Chem Lett* **16**, 4723-4727, doi:10.1016/j.bmcl.2006.07.008 (2006).

51   Cole, D. C. *et al.* Discovery of N1-(6-chloroimidazo[2,1-b][1,3]thiazole-5-sulfonyl)tryptamine as a potent, selective, and orally active 5-HT(6) receptor agonist. *J Med Chem* **50**, 5535-5538, doi:10.1021/jm070521y (2007).

Author contributions: TFR, CWM, AKC, DRB, PGS, MVH supervised and provided funding for these studies. MAB, CWM and TFR conceived the study and MAB and NB designed and carried out the screening experiments, with MGK, MP, LY, and JR assisting. MAB established image acquisition and analysis. EC and THN handled all compound transfers and provided robotics support. AKG provided chemistry support including quality control on key screening compounds. MVH provided software support. AKC and MVH curated data. MAB formally analyzed and prepared data for publication and MAB, NB, and CWM wrote and edited the manuscript, with contributions from all co-authors.

Competing interests: A provisional patent describing discovered active chemical matter has been filed.

List of Supplementary Materials:

Fig. S1: Effects of MOI on control compound EC_{50}s.

Tables S1: Anti-SARS-CoV-2 activities of known drugs and bioactive molecules identified as potent and selective hits in the pilot and ReFRAME screens.

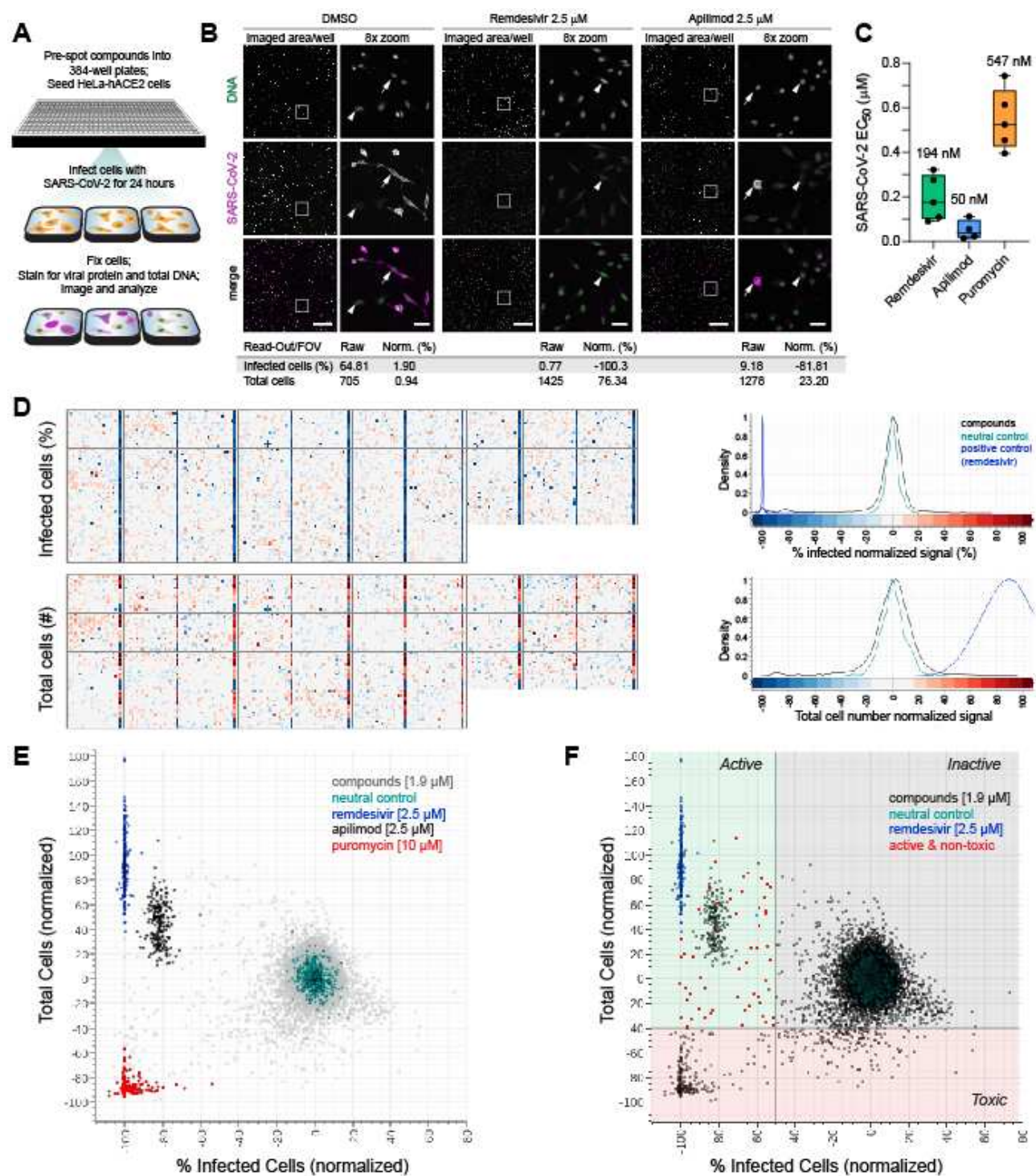| Read-Out/FOV	Raw	Norm. (%)		Raw	Norm. (%)		Raw	Norm. (%)
Infected cells (%)	64.81	1.90		0.77	-100.3		9.18	-81.81
Total cells	705	0.94		1425	76.34		1276	23.20

Fig. 1. A primary cell-based HCI assay identifies compounds active against SARS-CoV-2 infection. A) Simplified assay workflow. B) Representative images from dimethyl sulfoxide (DMSO)-, remdesivir- or apilimod-treated wells. The entire imaged area per well (4 fields of view taken with a 10× objective and stitched together) is shown for each treatment, as well as an 8-fold magnified segment demarcated with a white box. DNA signal [4′,6-diamidino-2-phenylindole (DAPI)] is colored green, and the virus visualized with immunofluorescence is colored magenta. Infected (arrow) and uninfected (arrowhead) cells are indicated; 500 µm and 50 µm scale bars are shown in the composite and magnified images, respectively. Raw and normalized (Norm.) values calculated from the images is shown. C) Box and whiskers plot of SARS-CoV-2 assay control EC_{50}s obtained from independent biological experiments with mean indicated with a bar and all data points shown. Whiskers indicate minimums and maximums. D) Heat map images of normalized data from 1.9 µM ReFRAME screening plates. Normalized activity values for % infected cells and total cell numbers are indicated according to the scale bar and density plot for compound and control wells is shown. DMSO-treated wells are in column 24 and positive control-treated wells (blocks of wells with 2.5 µM remdesivir, 2.5 µM apilimod, or 9.6 µM puromycin) in column 23. Density plots representing the frequency of values associated with each well type are shown on the right. E) Distribution of 1.9 µM ReFRAME screen data for compound and control wells. F) Screen hit selection thresholds.
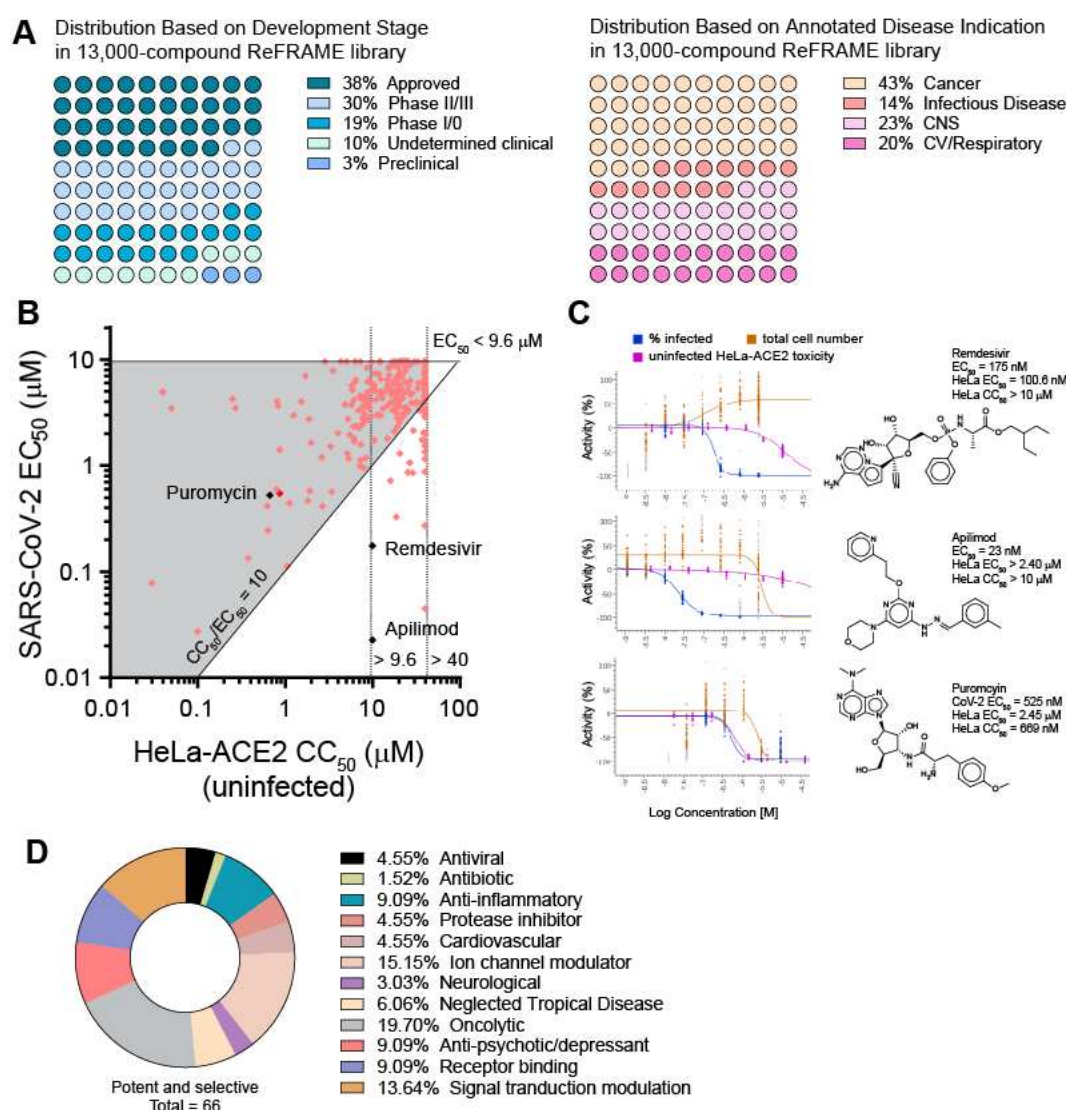
Fig. 2. Potent and selective compounds with anti-SARS-CoV-2 activity are identified in the ReFRAME library. A) The composition of the ReFRAME repurposing library with respect to clinical stage of development and disease indication. B) Dose response reconfirmation results, with the SARS-CoV-2 EC_{50} of each compound plotted against its host cell toxicity CC_{50} as assessed in uninfected HeLa-ACE2 cells. Dotted lines represent maximal concentrations tested in dose-response studies for the assay compounds (40 µM) and controls apilimod and remdesivir (10 µM). Activities of controls (black diamonds) and assay compounds (pink diamonds) are shown. Activity of the ReFRAME library copy of puromycin that was screened as part of this hit reconfirmation is also indicated (red diamond). C) SARS-CoV-2 EC_{50} (blue), infected HeLa-ACE2 EC_{50} (orange) and uninfected HeLa-ACE2 CC_{50} dose response curves for the remdesivir, apilimod and puromycin control compounds ran as part of ReFRAME hit reconfirmation. D) Classification of 66 potent and selective compounds according to their functional annotation.
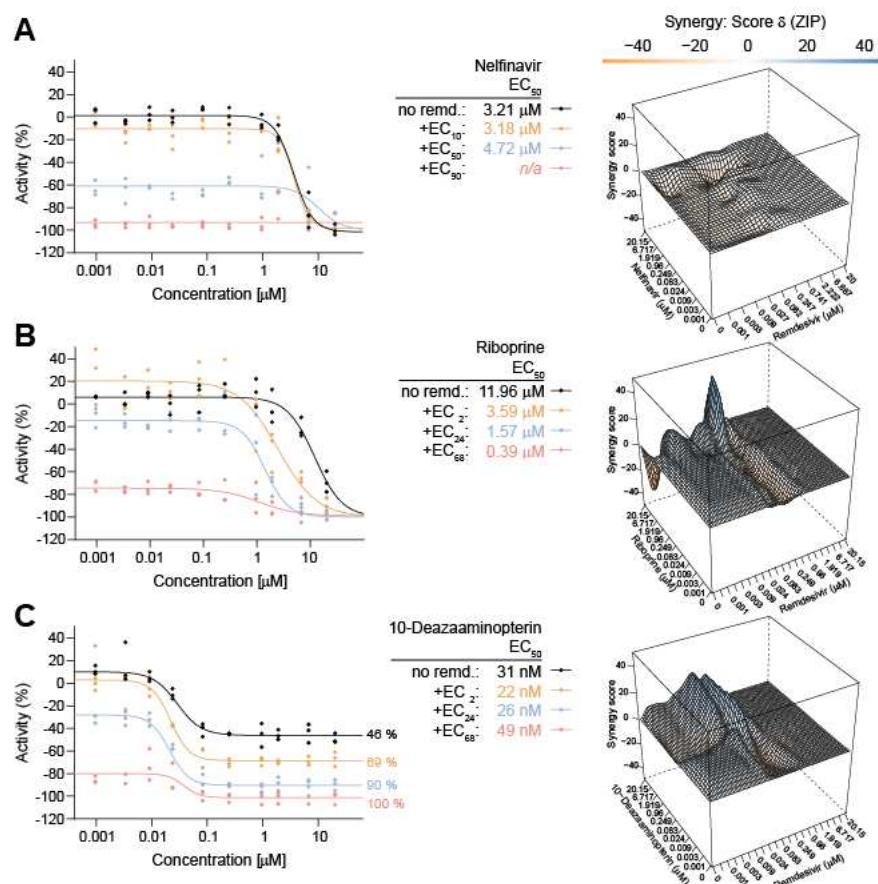
14

Figure 3. Anti-SARS-CoV-2 activity of drugs in combination with remdesivir showing additive and synergistic interactions. Dose response curves for nelfinavir (A), riboprine (B) and 10-deazaaminopterin (C) without or with increasing concentrations of remdesivir as well as the output of the synergy analysis, a 3-dimensional drug interaction landscape plotting synergy scores across all compound concentrations tested (median scores of 3 technical replicates) are shown. Additive effect: -$10 < \delta < 10$; synergistic effect: $\delta > 10$; antagonistic effect: $\delta < 10$. SARS-CoV-2 EC_{50} of each compound in combination with varying concentrations of remdesivir is also shown. Effective concentrations for remdesivir were calculated based on activity of remdesivir in each experiment.

Table 1. Primary and validation screen statistics.

Library	ReFRAME [1.9 µM]	ReFRAME [9.6 µM]	Total[b]
Compounds screened	11,861	11,861	11,861
Primary hits[a]	61	266	311
Average RZ'	0.8695	0.7241	0.7968
Hit rate	0.51%	2.24%	2.75%
Tested in dose response (DR)	60	265	310
$EC_{50} < 9.6$ µM	43	197	225
Reconfirmation rate	71.7%	74.3%	72.6%
$EC_{50} < 9.6$ µM, $CC_{50}/EC_{50} > 10$	8	41	45
Potent and selective hits	13.3%	15.5%	14.5%

[a] Primary hit thresholds: > 50 % inhibition of infection, < 40% cell toxicity; 6 border-line hits included in 1.9 µM

[b] non-overlapping hits from 1.9 and 9.6 µM screens

Table 2. Attractive reconfirmed hits with activity and selectivity against SARS-CoV-2

| Compound/Drug Name | Target/Mechanism | Clinical Stage | PK Exposure | | | SARS CoV-2 EC$_{50}$ (µM) | Uninfected HeLa-ACE2 CC$_{50}$ (µM) | Synergy score with remdesivir (δ) |
			Approx. C$_{max}$	Approx. t$_{1/2}$ (hours)	References			
Remdesivir (GS-5734)	RdRP inhibitor	Emergency FDA registration	5 µM (human oral)	1	23	0.194	> 10	n/a
Hydroxychloroquine	Antirheumatic drug	Registered	1.7 µM (human oral)	55	24	1.30	20.43	-1.572
Halofantrine HCl	Antimalarial; hemozoin inhibitor	Registered	1 µM (human oral)	58	25,26	0.33	18.71	-3.51
Amiodarone	Antiarrhythmic	Registered	6.8 µM (human oral)	100	27,28	1.53	> 40	0.68
Nelfinavir mesylate	HIV protease inhibitor	Registered	17 µM (human oral)	7	29,30	6.22	> 40	-1.23
Simeprevir	Hepatitis C NS3/4A protease inhibitor	Registered	32 µM (human oral)	16	31,32	7.82	> 40	-0.67
Manidipine	Ca^{2+}-channel blocker related to amlodipine	Registered	10 nM (human, oral)	3	33,34	7.97	> 40	-4.73
Ozanimod	S1P agonist	Registered	1.2 µM (human, oral)	20	35	4.98	> 40	-4.62
Osimertinib	EGFR (Thr790Met Mutant) Inhibitor	Registered	1.5 µM (human, oral)	50	36,37	1.71	> 40	n/d
Diclofensine	Dopamine reuptake inhibitor	Phase III	unk.; Generally low for class	n/d		6.06	> 40	n/d
Pancopride	5-HT3 antagonist	Phase III	300 nM (human, oral)	14	38	4.17	> 40	0.65
Apilimod	PIKfyve inhibitor	Phase II	600 nM (human, oral)	6	39	0.05	> 10	3.57
AQ-13	Malaria	Phase II	10 µM (human, oral)	350	40	1.07	26.6	-1.77
LY2228820	p38 inhibitor	Phase II	5 µM (human, oral)	190	41	1.75	36.61	n/d
MK-2206	Allosteric AKT inhibitor	Phase II	571 nM (human, oral)	80	42	2.02	> 40	2.09
R-428	AXL kinase inhibitor	Phase II	750 nM (oral, humans)	90	43	2.88	> 40	7.22
Hanfangchin A	Ca^{2+}-channel blocker	Phase I	0.5 µM (rat, oral)	21	44	0.72	16.09	-3.61
L 796568	Beta-3 adrenergic receptor agonist	Phase I	0.3 µM (dog, oral)	13	45,46	1.15	> 40	3.16
NCO 700	Cathepsin B inhibitor	Phase I	unk.	unk.		1.16	> 40	0.21
SMN-C3	SMA splicing modifier	Phase I	Generally high for class; 2 µM (mouse, oral)	10	47	2.00	> 40	-0.37
GS-9901	Phosphatidylinositol 3-kinase delta inhibitor	Phase I	1.8 µM (rat, oral)	2	48	4.13	> 40	n/d
GW-803430	Melanin-Concentrating Hormone MCH-R1 (SLC-1) Receptor Antagonist	Phase I	585 nM (rat, mouse oral)	11	49,50	4.62	> 40	n/d
SAX-187	5 Hydroxytryptamine 6 receptor agonist	Phase I	0.4 µM (rat, oral)	3	51	5.35	> 40	-2.98
YM-161514	Ca-channel blocker	Phase I	unk.; Generally low for class	unk.		4.53	> 40	0.60
Dutacatib	Cathepsin K inhibitor	Discovery	unk.	unk.		3.48	> 40	2.95
KC 11404	Lipoxygenase 5 inhibitor	Discovery	unk.	unk.		4.41	> 40	-2.82
NNC 090026	Sodium and calcium channel inhibitor	Discovery	unk.	unk.		7.34	> 40	n/d

C$_{max}$, maximum serum concentration; t$_{1/2}$, time to half C$_{max}$; t$_{max}$, time to C$_{max}$;
unk., unknown; *n/a,* not applicable; *n/d,* not determined